Structure and mechanism of turbulence under dynamical restriction in plane Poiseuille flow

Brian F. Farrell[1], Petros J. Ioannou†[2], Javier Jiménez[3], Navid C. Constantinou[4], Adrián Lozano-Durán[3] and Marios-Andreas Nikolaidis[2]

[1]Department of Earth and Planetary Sciences, Harvard University, Cambridge, MA 02138, USA

[2]Department of Physics, National and Kapodistrian University of Athens, Panepistimiopolis, Zografos, Athens, 15784, Greece

[3]School of Aeronautics, Universidad Politécnica de Madrid, 28040, Madrid, Spain

[4]Scripps Institution of Oceanography, UC San Diego, La Jolla, CA 92037-0213, USA

The perspective of statistical state dynamics (SSD) has recently been applied to the study of mechanisms underlying turbulence in a variety of physical systems. An example application of SSD is that of the second order closure, referred to as stochastic structural stability theory (S3T), which has provided insight into the dynamics of wall turbulence and specifically the emergence and maintenance of the roll/streak structure. When implemented as a coupled set of equations for the streamwise mean and perturbations, this closure eliminates nonlinear interactions among the perturbations restricting nonlinearity in the dynamics to that of the mean equation and interaction between the mean and perturbations. Simulations at modest Reynolds numbers reveal that the essential features of wall-turbulence dynamics are retained with the dynamics restricted in this manner. Here this restriction of the dynamics is used to obtain a closely related dynamical system, referred to as the restricted non-linear (RNL) system, which is used to study the structure and dynamics of turbulence in plane Poiseuille flow at moderately high Reynolds numbers. Remarkably, the RNL system spontaneously limits the support of its turbulence to a small set of streamwise Fourier components giving rise to a natural minimal representation of its turbulence dynamics. Although greatly simplified, this RNL turbulence exhibits natural-looking structures and statistics. Surprisingly, even when a further truncation of the perturbation support to a single streamwise component is imposed the RNL system continues to produce self-sustaining turbulent structure and dynamics. The turbulent flow in RNL simulations at the Reynolds numbers studied is dominated by the roll/streak structure in the buffer layer and very-large-scale structure (VLSM) in the outer layer. In this work diagnostics of the structure, spectrum and energetics of RNL and DNS turbulence are used to demonstrate that the roll/streak dynamics supporting the turbulence in the buffer and logarithmic layer is essentially similar in RNL and DNS.

1. Introduction

Turbulence in wall-bounded shear flow is maintained by transfer of kinetic energy from the forced flow to perturbations. If the forced flow is inflectional then fast hydrodynamic linear instabilities are available to provide the mechanism for this transfer. However,

† Email address for correspondence: pjioannou@phys.uoa.gr

most wall-bounded shear flows such as those in channels or pipes are not inflectional and the mechanism of energy transfer to the perturbations involves nonlinear processes that exploit the non-normality of the flow dynamics to produce sustained transfer of energy from the mean to the perturbations. Mechanisms proposed to effect this transfer we refer to collectively as self-sustaining processes (SSP). These mechanisms have in common exploiting non-normal transient growth by nonlinearly destabilizing the optimal roll/streak structure resulting in sustained transfer of energy to the perturbations (Farrell & Ioannou 2012). The fundamental importance of the roll/streak structure in the dynamics of wall-turbulence was first inferred after it was observed in the near wall region in boundary layer flows by the use of hydrogen bubbles (Kline *et al.* 1967) and seen in the early direct numerical simulations (DNS) of channel flows (cf. Kim *et al.* (1987)). Recently, in both experiments and numerical simulations of turbulent flows at high Reynolds numbers, roll/streak structures have been identified in the logarithmic layer with self-similar structure scaling with the distance from the wall (del Álamo *et al.* 2006; Lozano-Durán *et al.* 2012; Lozano-Durán & Jiménez 2014b). Higher in the flow similar very large streaky structures are seen that scale with the channel half-height or pipe radius, h, or with the boundary layer thickness δ (Bullock *et al.* 1978; Jiménez 1998; Kim & Adrian 1999). These are variously referred to as global modes, superstructures or very large-scale motions (VLSM) (del Álamo *et al.* 2004; Toh & Itano 2005; Hutchins & Marusic 2007; Marusic *et al.* 2010). The streamwise extent of the VLSM has been estimated from cross-spectral analysis to be of the order of $30h$ in pipe flows and of the order of $10 - 15\delta$ in boundary layer flows (Jiménez & Hoyas 2008; Hellström *et al.* 2011), but Hutchins & Marusic (2007) argue that these are underestimates of their actual length. In recent DNS simulations of turbulent channels at $Re_\tau = 550$ Lozano-Durán & Jiménez (2014a) determined that VLSM structures extended to $30h$.

Statistical state dynamics (SSD) has provided a new perspective on the nonlinear instability of the SSP operating in wall-turbulence by employing a second order closure of the equations governing the cumulants of the full SSD (Farrell & Ioannou 2012). This closure, referred to as S3T, had been used previously to study large-scale coherent structure dynamics in planetary turbulence (Farrell & Ioannou 2003, 2007, 2008, 2009a; Marston *et al.* 2008; Srinivasan & Young 2012; Bakas & Ioannou 2013; Constantinou *et al.* 2014a, 2015; Parker & Krommes 2014) and drift-wave turbulence in plasmas (Farrell & Ioannou 2009b; Parker & Krommes 2014). At low Reynolds numbers the S3T closure of wall-bounded turbulence maintains a self-sustained turbulent state that has been comprehensively analyzed (Farrell & Ioannou 2012). The dynamic interactions retained in S3T are restricted to those between the mean (defined as flow components with streamwise wavenumber $k_x = 0$) and perturbations (defined as flow components with streamwise wavenumber $k_x \neq 0$) with nonlinearity retained only in the mean equations. Restriction of Navier–Stokes (NS) dynamics in this way produces the RNL (Restricted Nonlinear) approximation to NS. Because the perturbation-perturbation interactions have been neglected in the perturbation equation, RNL/S3T does not support a classical turbulent cascade. Further, in this work RNL will be regarded as an approximation to the SSD of S3T in which a single member of the infinite ensemble retained in S3T is used to calculate the second order statistics. One consequence of this formulation is that phase information is not retained for the perturbation fields, only their second order correlations being relevant to this second order SSD. While approximating the second order statistics as an RNL has the advantage over S3T that it can be easily implemented at high resolution and the resulting simulations can be compared to DNS providing insight into the dynamics of turbulence (cf. Thomas *et al.* (2014); Constantinou *et al.* (2014b)).

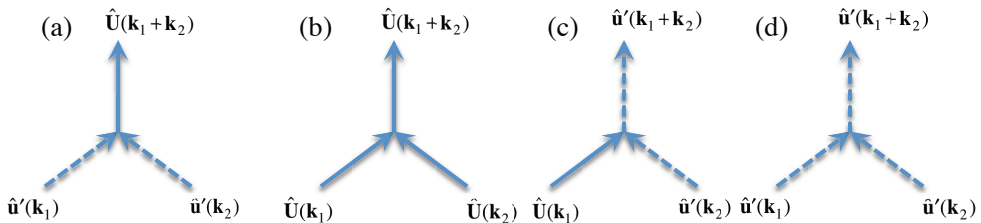In this paper, turbulent simulations using RNL and DNS at relatively high Reynolds

Figure 1: Nonlinear interactions that are included or excluded in the RNL approximation of the NS equations. Mean flow Fourier components $\hat{\mathbf{U}}(\mathbf{k})$ with wavenumber $\mathbf{k} = (0, k_y, k_z)$ are indicated with solid arrows, the perturbation Fourier components $\hat{\mathbf{u}}'(\mathbf{k})$ with $k_x \neq 0$ with dashed arrows. The possible nonlinear interactions are: (a) a perturbation with streamwise wavenumber k_{x1} interacts with another perturbation with $k_{x2} = -k_{x1}$ to produce a mean flow component with $k_x = 0$, (b) two mean flow components interact to make another mean flow component, (c) a mean flow component interacts with a perturbation to make a perturbation component and (d) two perturbation components with streamwise wavenumbers $k_{x1} \neq -k_{x2}$ interact to make another perturbation component. All interactions are included in the NS equations (2.1). Interactions (a) and (b) are included in the RNL mean equations (2.3a), while in the RNL perturbation equations (2.3b) only interactions (c) are included.

numbers in pressure driven channel flow are compared. Included in this comparison are flow statistics, structures, and dynamical diagnostics. This comparison allows the effects of the dynamical restriction in the S3T closure to be studied at these moderately high Reynolds numbers for which exact closure using a fully converged second cumulant is not numerically feasible.

We find that the highly simplified RNL dynamics supports a self-sustaining roll/streak SSP in the buffer layer similar to that of DNS and that roll/streak structures in the log-layer are also supported by an essentially similar SSP. Because of the dynamical restrictions inherent in RNL, by necessity this SSP is sustained by the non-normal parametric nonlinear instability mechanism previously identified by using S3T to maintain perturbation variance in Couette flow at low Reynolds number (Farrell & Ioannou 2012). Similar to the SSP identified in Couette flow using S3T, this roll/streak structure has zero streamwise wavenumber. It follows that nonzero streamwise wavenumbers observed in association with RNL turbulence do not indicate a fundamental limitation of the streamwise extent of the streak underlying RNL turbulence. Because $k_x \neq 0$ perturbations may be of large amplitude, observation may suggest that the underlying roll/streak structure has nonzero wavenumber (Hutchins & Marusic 2007) but in RNL this is by definition not the case. Moreover, in this work we provide evidence closely relating NS turbulence in its dynamics to RNL turbulence. Because the dynamics of RNL turbulence can be understood fundamentally from its direct relation with S3T turbulence these results support the conclusion that the mechanism responsible for the large scale structure seen in wall-bounded turbulence in moderate Reynolds number flow is the same in S3T, RNL and DNS: the roll/streak/perturbation SSP that was previously identified in S3T turbulence.

2. RNL Dynamics

Consider a plane Poiseuille flow in which a constant mass flux is maintained by application of a time-dependent pressure, $G(t)x$, where x is the streamwise coordinate. The wall-normal direction is y and the spanwise direction is z. The lengths of the channel in the streamwise, wall-normal and spanwise direction are respectively L_x, $2h$ and L_z. The channel walls are at $y/h = 0$ and 2. Averages are denoted by square brackets with a subscript denoting the variable which is averaged, i.e. spanwise averages by $[\,\cdot\,]_z = L_z^{-1} \int_0^{L_z} \cdot \; \mathrm{d}z$, time averages by $[\,\cdot\,]_t = T^{-1} \int_0^T \cdot \; \mathrm{d}t$, with T sufficiently long. Multiple subscripts denote an average over the subscripted variables in the order they appear, i.e. $[\,\cdot\,]_{x,y} \equiv [[\,\cdot\,]_x]_y$. The velocity, $\mathbf{u}$, is decomposed into its streamwise mean value, denoted by $\mathbf{U}(y, z, t) \equiv [\mathbf{u}(x, y, z, t)]_x$, and the deviation from the mean (the perturbation), $\mathbf{u}'(x, y, z, t)$, so that $\mathbf{u} = \mathbf{U} + \mathbf{u}'$. The pressure gradient is similarly written as $\nabla p = \nabla\left(-G(t)x + P(y, z, t) + p'(x, y, z, t)\right)$. The NS decomposed into an equation for the mean and an equation for the perturbation are:

$$\partial_t \mathbf{U} + \mathbf{U} \cdot \nabla \mathbf{U} - G(t)\hat{\mathbf{x}} + \nabla P - \nu \Delta \mathbf{U} = -\left[\mathbf{u}' \cdot \nabla \mathbf{u}'\right]_x \; , \qquad (2.1a)$$

$$\partial_t \mathbf{u}' + \mathbf{U} \cdot \nabla \mathbf{u}' + \mathbf{u}' \cdot \nabla \mathbf{U} + \nabla \mathbf{p}' - \nu \Delta \mathbf{u}' = -\left(\mathbf{u}' \cdot \nabla \mathbf{u}' - \left[\mathbf{u}' \cdot \nabla \mathbf{u}'\right]_x\right) \; , \qquad (2.1b)$$

$$\nabla \cdot \mathbf{U} = 0 \; , \quad \nabla \cdot \mathbf{u}' = 0 \; , \qquad (2.1c)$$

where ν is the coefficient of kinematic viscosity. Nonlinear interactions among the mean flow components (flow components with streamwise wavenumber $k_x = 0$) and perturbations (flow components with streamwise wavenumber $k_x \neq 0$) in (2.1) are summarized in Fig. 1 The x, y, z components of $\mathbf{U}$ are (U, V, W) and the corresponding components of $\mathbf{u}'$ are (u', v', w'). Streamwise mean perturbation Reynolds stress components are denoted as e.g. $[u'u']_x$, $[u'v']_x$.

The streak component of the streamwise mean flow is denoted by U_s and defined as

$$U_s \equiv U - [U]_z \; . \qquad (2.2)$$

The V and W are the streamwise mean velocities of the roll vortices. We also define the streak energy density, $E_s = h^{-1} \int_0^h \mathrm{d}y \, \frac{1}{2} \left[U_s^2\right]_z$, and the roll energy density, $E_r = h^{-1} \int_0^h \mathrm{d}y \, \frac{1}{2} \left[(V^2 + W^2)\right]_z$.

The RNL approximation is obtained by neglecting the perturbation–perturbation interaction terms in (2.1b) (cf. Fig. 1). The RNL system is:

$$\partial_t \mathbf{U} + \mathbf{U} \cdot \nabla \mathbf{U} - G(t)\hat{\mathbf{x}} + \nabla P - \nu \Delta \mathbf{U} = -\left[\mathbf{u}' \cdot \nabla \mathbf{u}'\right]_x \; , \qquad (2.3a)$$

$$\partial_t \mathbf{u}' + \mathbf{U} \cdot \nabla \mathbf{u}' + \mathbf{u}' \cdot \nabla \mathbf{U} + \nabla \mathbf{p}' - \nu \Delta \mathbf{u}' = 0 \; , \qquad (2.3b)$$

$$\nabla \cdot \mathbf{U} = 0 \; , \quad \nabla \cdot \mathbf{u}' = 0 \; . \qquad (2.3c)$$

Equation (2.3a) describes the dynamics of the streamwise mean flow, $\mathbf{U}$, which is driven by the divergence of the streamwise mean perturbation Reynolds stresses. These Reynolds stresses are obtained from (2.3b) in which the streamwise varying perturbations, $\mathbf{u}'$, evolve under the influence of the time dependent streamwise mean flow $\mathbf{U}(y, z, t)$ with no explicitly retained interaction among these streamwise varying perturbations (the retained interactions are shown in the diagram of Fig. 1). Remarkably, RNL self-sustains turbulence solely due to the perturbation Reynolds stress forcing of the streamwise mean flow (2.3a), in the absence of which a self-sustained turbulent state cannot be established (Gayme 2010; Gayme *et al.* 2010).

Because the RNL equations do not include interactions among the perturbations and because $\mathbf{U}$ is streamwise constant each component $\hat{\mathbf{u}}'_{k_x} e^{ik_x x}$ of perturbation velocity $\mathbf{u}'$ in

Abbreviation	$[L_x, L_z]/h$	$N_x \times N_z \times N_y$	Re_τ	$[L_x^+, L_z^+]$
NS950	$[\pi , \pi/2]$	$256 \times 255 \times 385$	939.9	[2953, 1476]
RNL950	$[\pi , \pi/2]$	$256 \times 255 \times 385$	882.4	[2772, 1386]
RNL950k_x12	$[\pi , \pi/2]$	$3 \times 255 \times 385$	970.2	[3048, 1524]

Table 1: Simulation parameters. $[L_x, L_z]/h$ is the domain size in the streamwise and spanwise direction. N_x, N_z are the number of Fourier components after dealiasing and N_y is the number of Chebyshev components. Re_τ is the Reynolds number of the simulation based on the friction velocity and $[L_x^+, L_z^+]$ is the channel size in wall units. The Reynolds number based on the bulk velocity is $Re = U_b h/\nu = 18511$ in all cases.

the Fourier expansion:

$$\mathbf{u}'(x,y,z,t) = \sum_{k_x} \hat{\mathbf{u}}'_{k_x}(y,z,t)\, e^{ik_x x} \ , \tag{2.4}$$

with $k_x = \pm(2\pi/L_x)[1,2,3,\ldots,N_x/2]$, evolves independently in (2.3b) and equations (2.3b) can be split into independent equations for each k_x. By taking the Fourier transform of (2.3b) in x and eliminating the perturbation pressure, equations (2.3b) can be symbolically written as:

$$\partial_t \hat{\mathbf{u}}'_{k_x} = \mathbf{A}_{k_x}(\mathbf{U})\,\hat{\mathbf{u}}'_{k_x} \ , \tag{2.5}$$

with

$$\mathbf{A}_{k_x}(\mathbf{U})\,\hat{\mathbf{u}}'_{k_x} = \mathbf{P}_L \left(-\mathbf{U}\cdot\nabla_{k_x}\hat{\mathbf{u}}'_{k_x} - \hat{\mathbf{u}}'_{k_x}\cdot\nabla_{k_x}\mathbf{U} + \nu\Delta_{k_x}\hat{\mathbf{u}}'_{k_x} \right) \ , \tag{2.6}$$

and $\mathbf{P}_L$ is the Leray projection enforcing non-divergence of the k_x Fourier components of the perturbation velocity field with $\nabla_{k_x} \equiv (ik_x, \partial_y, \partial_z)$ and $\Delta_{k_x} \equiv \partial_y^2 + \partial_z^2 - k_x^2$ (Foias *et al.* 2001). The RNL system can then be written in the form:

$$\partial_t \mathbf{U} + \mathbf{U}\cdot\nabla\mathbf{U} - G(t)\hat{\mathbf{x}} + \nabla P - \nu\Delta\mathbf{U} = -\frac{1}{2}\sum_{k_x \in K_x} \mathrm{Re}\left[\partial_y(\hat{v}'_{k_x}\hat{\mathbf{u}}'^*_{k_x}) + \partial_z(\hat{w}'_{k_x}\hat{\mathbf{u}}'^*_{k_x}) \right] \ , \tag{2.7a}$$

$$\partial_t \hat{\mathbf{u}}'_{k_x} = \mathbf{A}_{k_x}(\mathbf{U})\,\hat{\mathbf{u}}'_{k_x} \ , \quad k_x \in K_x \ , \tag{2.7b}$$

$$\nabla \cdot \mathbf{U} = 0 \ , \tag{2.7c}$$

with K_x the positive k_x wavenumbers $2\pi/L_x[1,2,3,\ldots,N_x/2]$ included in the simulation and $*$ in (2.7a) denoting complex conjugation.

3. DNS and RNL Simulations

The data were obtained from a DNS of (2.1) and from an RNL simulation, governed by (2.3), that is directly associated with the DNS. Both the DNS and its directly associated RNL are integrated with no-slip boundary conditions in the wall-normal direction and periodic boundary conditions in the streamwise and spanwise directions. The dynamics were expressed in the form of evolution equations for the wall-normal vorticity and the Laplacian of the wall-normal velocity, with spatial discretization and Fourier dealiasing in the two wall-parallel directions and Chebychev polynomials in the wall-normal direction (Kim *et al.* 1987). Time stepping was implemented using the third-order semi-implicit Runge-Kutta method.

The geometry and resolution of the DNS and RNL simulations is given in Table 1. Quantities reported in outer units lengths are scaled by the channel half-width, h, and time by h/u_τ and the corresponding Reynolds number is $Re_\tau = u_\tau h/\nu$ where $u_\tau = \sqrt{\nu \, dU/dy|_\mathrm{w}}$ ($dU/dy|_\mathrm{w}$ is the shear at the wall) is the friction velocity. Inner units lengths are scaled by $h_\tau = Re_\tau^{-1} h$ and time by $Re_\tau^{-1} h/u_\tau$. Velocities scaled by the friction velocity u_τ will be denoted with the superscript $+$, which indicates inner unit scaling.

We report results from three simulations: a DNS simulation, denoted NS950, with $Re_\tau \approx 940$, the corresponding RNL simulation, denoted RNL950 and a constrained RNL simulation, denoted RNL950k_x12. Both RNL simulations were initialized with an NS950 state and run until a steady state was established. In RNL950k_x12 only the single streamwise Fourier component with wavenumber $k_x h = 12$ was retained in (2.7b) by limiting the spectral components of the perturbation equation to only this streamwise wavenumber; this simulation self-sustained a turbulent state with $Re_\tau = 970.2$. In RNL950 the number of streamwise Fourier components was not constrained; this simulation self-sustained a turbulent state at $Re_\tau = 882.2$.

We show in Fig. 2 the transition from NS950 to RNL950 turbulence. The NS950 is switched at time $tu_\tau/h = 100$ to an RNL950 simulation by suppressing the perturbation-perturbation interactions, represented by the r.h.s. in equation (2.1b). The transition from DNS to RNL is evident in the time series of the energy density

$$E_{k_x} = (hL_z)^{-1} \int_0^h \mathrm{d}y \int_0^{L_z} \mathrm{d}z \, \left| \hat{\mathbf{u}}'_{k_x} \right|^2 \ , \qquad (3.1)$$

of the streamwise Fourier components of the perturbation field. The time evolution of the energy density of the first 15 streamwise Fourier components, with wavenumbers $hk_x = 2, 4, \ldots, 30$, in NS950 and in RNL950 is shown in Fig. 2a. In NS950, all k_x components maintain non-zero energy density. After the transition asymptotically the dynamics of the RNL950 turbulence is maintained by interaction between the set of 6 surviving wavenumbers, $hk_x = 2, 4, \ldots, 12$ and the $k_x = 0$ component of the flow (cf. Fig. 2a). The result of restriction of NS dynamics to RNL is thus a spontaneous reduction in the support of the turbulence in streamwise Fourier components with all Fourier components having wavelength smaller than $\pi h/6$ ($hk_x > 12$) decaying exponentially producing a reduced complexity dynamics in which turbulence self-sustains on this greatly restricted support in streamwise Fourier harmonics. We view this transition of NS950 turbulence to RNL950 turbulence as revealing the set of structures that are naturally involved in maintaining the turbulent state. Given this spontaneous complexity reduction the question arises: how few streamwise varying perturbation components are required in order to self-sustain RNL turbulence at this Reynolds number? We show in RNL950k_x12 that even if we retain only the single perturbation component with wavelength $\pi h/6$ ($hk_x = 12$) a realistic self-sustained turbulent state persists†.

4. RNL as a minimal turbulence model

We have seen that as a result of its dynamical restriction, RNL turbulence is supported by a small subset of streamwise Fourier components. In order to understand this property of RNL dynamics consider that the time dependent streamwise mean state of a turbulent RNL simulation has been stored, so that the mean flow field $\mathbf{U}(y, z, t)$ is known at each instant. Then each k_x component of the perturbation flow field that is retained in the

† For a discussion of the streanwise wavenumber support of RNL turbulence cf. Thomas *et al.* (2015).
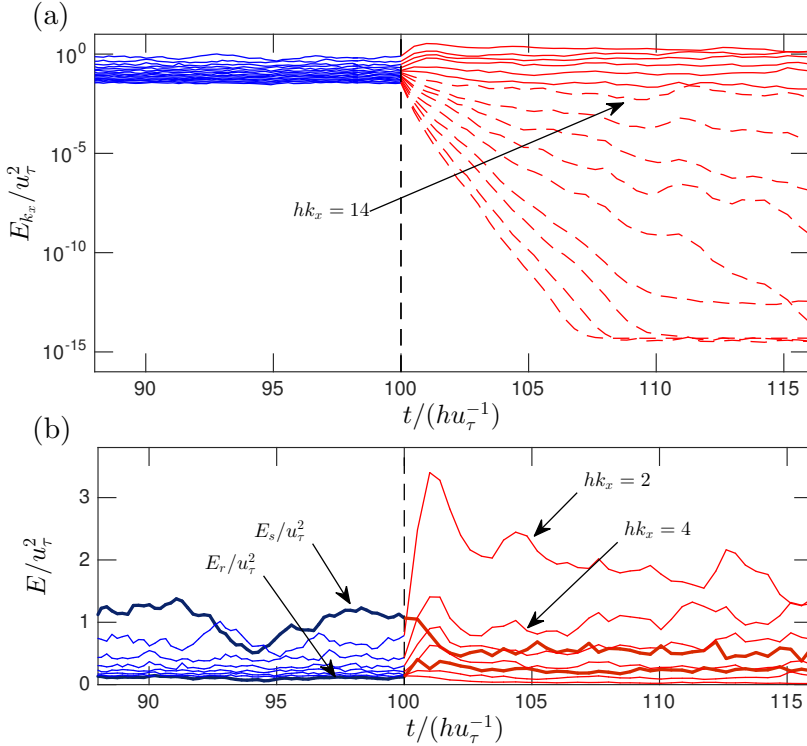
Figure 2: An NS950 simulation up to $t/(hu_\tau^{-1}) = 100$ (indicated with the vertical line) is continued subsequently under RNL dynamics. (a) The energy density, E_{k_x}, of the first 15 streamwise varying Fourier components ($hk_x = 2, 4, \ldots, 30$). The energy density of the Fourier components decreases monotonically with increasing wavenumber. Decaying Fourier components are indicated with dashed lines. After the transition to RNL dynamics all components with $hk_x \geqslant 14$ decay ($hk_x = 14$ decays, although it is not apparent until later times than shown in this figure). Asymptotically the dynamics of the RNL950 turbulence is maintained by interaction between the set of surviving $hk_x = 2, 4, \ldots, 12$ Fourier components and the mean flow ($k_x = 0$). (b) Detailed view showing the energy density of the mean and surviving perturbation components during the transition from NS to RNL dynamics, in which the total energy increased by 10%. For the $k_x = 0$ shown are: the streak energy density, E_s, and roll energy density, E_r. The energy density of the $hk_x = 2, 4, 6, 8$ components increases rapidly during the adjustment after transition to RNL dynamics. Note that the total energy density in the perturbation $k_x \neq 0$ components decreases from $0.91u_\tau^2$ in the NS950 ($0.56u_\tau^2$ being in the components that survive in the RNL) to $0.78u_\tau^2$ in RNL950. Also the roll/streak energy density decreases from $1.1u_\tau^2$ in NS950 to $0.8u_\tau^2$ in RNL950, while the energy density of the $k_x = k_z = 0$ component increases from $397u_\tau^2$ to $448u_\tau^2$.

RNL evolves according to (2.7b):

$$\partial_t \hat{\mathbf{u}}'_{k_x} = \mathbf{A}_{kx}(\mathbf{U}) \, \mathbf{u}'_{k_x} \ , \tag{4.1}$$

with $\mathbf{A}_{k_x}(\mathbf{U})$ given by (2.6).

With the time dependent mean flow velocity $\mathbf{U}$ obtained from a simulation of a

turbulent state imposed, equations (4.1) are time dependent linear equations for $\hat{\mathbf{u}}'_{k_x}$ with the property that each k_x streamwise component of the perturbation state of the RNL, $\hat{\mathbf{u}}'_{k_x}$, can be recovered with exponential accuracy (within an amplitude factor and a phase) by integrating forward (4.1) regardless of the initial state. This follows from the fundamental property of time dependent systems that all initial states, $\hat{\mathbf{u}}_{k_x}(y, z, t = 0)$, converge eventually with exponential accuracy to the same structure. In fact, each of the $\hat{\mathbf{u}}'_{k_x}$ assumes the unique structure of the top Lyapunov vector associated with the maximum Lyapunov exponent of (4.1) at wavenumber k_x,

$$\lambda_{k_x} = \limsup_{t \to \infty} \frac{\log \|\hat{\mathbf{u}}'_{k_x}(y, z, t)\|}{t} \ , \tag{4.2}$$

where $\| \cdot \|$ is any norm of the velocity field (cf. Farrell & Ioannou (1996)). Moreover, for each k_x this top Lyapunov exponent has the further property of being either exactly zero or negative with those structures having $\lambda_{k_x} = 0$ supporting the perturbation variance. Vanishing of the maximum Lyapunov exponent of the perturbation system is required for it to constitute a component of the turbulence state trajectory, as exactly zero Lyapunov exponent is necessary in order that the perturbation state variance be finite and nonzero (Farrell & Ioannou 2012).

This property of RNL turbulence being sustained by the top Lyapunov perturbation structures implies that the perturbation structure contains only the streamwise varying perturbation Fourier components, k_x, that are contained in the support of these top Lyapunov structures with $\lambda_{k_x} = 0$ (cf. Farrell & Ioannou (2012)). It is remarkable that only 6 Fourier components, k_x, are contained in the support of RNL950 and even more remarkable that the RNL SSP persists even when this naturally reduced set is further truncated to a single streamwise Fourier component, as demonstrated in RNL950k_x12. This result was first obtained in the case of self-sustained Couette turbulence at low Reynolds numbers (cf. Farrell & Ioannou (2012); Farrell *et al.* (2012)).

This vanishing of the Lyapunov exponent associated with each streamwise wavenumber is enforced in RNL by the nonlinear feedback process acting between the streaks and the perturbations by which the parametric instability of the perturbations is suppressed at sufficiently high streak amplitude so that the instability maintains in the asymptotic limit zero Lyapunov exponent.

5. Comparison between NS and RNL turbulence structure and dynamics

In this section we compare turbulence diagnostics obtained from self-sustaining turbulence in the RNL system (2.3), to diagnostics obtained from a parallel associated DNS of (2.1) (cf. Table 1 for the parameters). The corresponding turbulent mean profiles for the NS950 and the RNL950 and RNL950k_x12 simulations are shown in Fig. 3.

Previous simulations in Couette turbulence (Thomas *et al.* 2014) at lower Reynolds numbers ($Re_\tau = 65$) showed very small difference between the mean turbulent profile in NS and RNL simulations. These simulations at larger Reynolds numbers show significant differences in the mean turbulent profiles sustained by NS950 and RNL950 simulations. This is especially pronounced in the outer regions where RNL950 sustains a mean turbulent profile with substantially smaller shear.

All these examples exhibit a logarithmic layer. However, the shear in these logarithmic regions are different: the von Kármán constant of NS at $Re_\tau = 950$ is $\kappa = 0.4$ while for the RNL950 it is $\kappa = 0.77$ and for the RNL950k_x12 it is $\kappa = 0.53$. Formation of a logarithmic layer indicates that the underlying dynamics of the logarithmic layer are
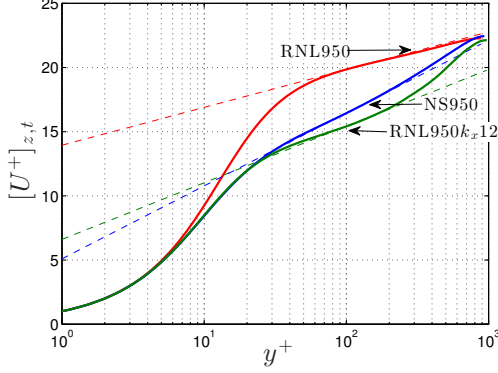
Figure 3: Streamwise velocity $[U^+]_{z,t}$ for the simulations listed in table 1. Shown are the corresponding profiles in wall units. The dashed lines indicate the best fit to the law of the wall, $[U^+(y)]_{z,t} = (1/\kappa) \log(y^+) + C$, with coefficients: $\kappa = 0.40$, $C = 5.1$ for NS950, $\kappa = 0.77$, $C = 14.0$ for RNL950 and $\kappa = 0.53$, $C = 6.6$ for RNL950k_x12.
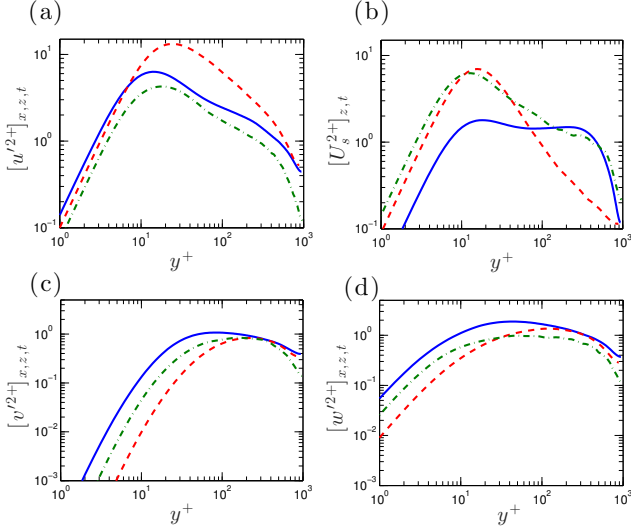

Figure 4: Comparison of velocity fluctuations for the simulations listed in table 1. Shown are (a): $[u'^{2+}]_{x,z,t}$, (b): $[U_s^{2+}]_{z,t}$, (c): $[v'^{2+}]_{x,z,t}$, (d): $[w'^{2+}]_{x,z,t}$ for NS950 (solid), RNL950 (dashed) and RNL950k_x12 (dash-dot).

retained in RNL. Because in the logarithmic layer RNL dynamics maintains in local balance with dissipation essentially the same stress and variance as NS but with a smaller shear, RNL dynamics is in this sense more efficient than NS in that it produces the same local Reynolds stress while requiring less local energy input to the turbulence. To see this consider that local energy balance in the log-layer requires that the energy production, $U'u_\tau^2$, (with $U' \equiv d[U]_{z,t}/dy$) equals the energy dissipation ϵ, and because in the log-layer $U' = u_\tau/\kappa y$, local balance requires that $u_\tau^3/(\kappa y) = \epsilon$, as discussed by Townsend (1976); Dallas *et al.* (2009), which indicates that the higher κ in RNL simulations at the same u_τ is associated with smaller dissipation. In RNL dynamics this local equilibrium determining the shear and by implication κ results from establishment of a statistical equilibrium

(a)

(b)
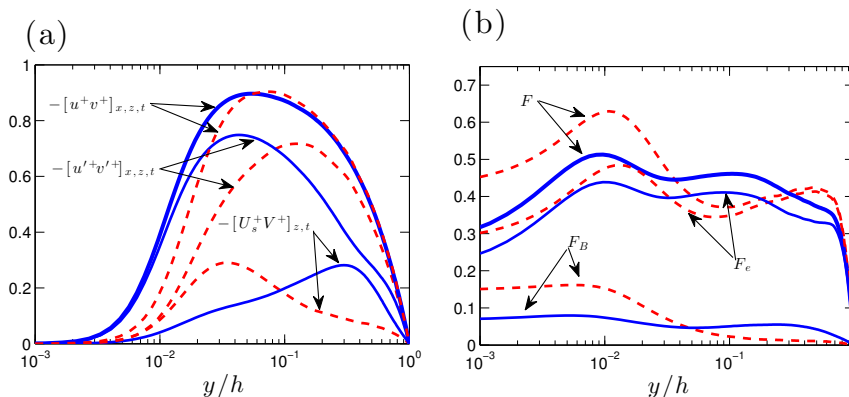

Figure 5: (a): The Reynolds stress component, $-[uv]_{x,z,t}$ in NS950 (solid) and in RNL950 (dashed). Also shown are each of the terms, $-[U_sV]_{z,t}$ and $-[u'v']_{x,z,t}$ that sum to $-[uv]_{x,z,t}$. Although the NS and RNL values of the total $-[uv]_{x,z,t}$ are almost identical, the contribution of $-[U_sV]_{z,t}$ and $-[u'v']_{x,z,t}$ differ in NS and RNL. (b): Structure coefficient, F, in NS950 (solid) and in RNL950 (dashed). Shown are $F_B = -[UV]_{z,t}\big/\sqrt{[U^2]_{z,t}[V^2]_{z,t}}$, $F_e = -[u'v']_{x,z,t}\big/\sqrt{[u'^2]_{x,z,t}[v'^2]_{x,z,t}}$ and $F = -[uv]_{x,z,t}\big/\sqrt{[u^2]_{x,z,t}[v^2]_{x,z,t}}$.

by the feedback between the perturbation equation and the mean flow equation, with this feedback producing a κ determined to maintain energy balance locally in y. These considerations imply that the κ observed produces a local shear for which, given the turbulence structure which is influenced by the restricted set of retained Fourier structures in RNL, the Reynolds stress and dissipation are in local balance.

Examination of the transition from NS950 to RNL950, shown by the simulation diagnostics in Fig. 2b, reveals the action of this feedback control associated with the reduction in shear of the mean flow. When in (2.1b) the interaction among the perturbations is switched off, so that the simulation is governed by RNL dynamics, an adjustment occurs in which the energy of the surviving $k_x \neq 0$ components obtain new statistical equilibrium values. Initial increase of the energy of these components is expected because the dissipative effect of the perturbation–perturbation nonlinearity that acts on these components is removed in RNL. As these modes grow, the SSP cycle adjusts to establish a new turbulent equilibrium state which is characterized by increase in energy of the largest streamwise scales and reduced streak amplitude. In the outer layer this new equilibrium is characterized in the case of RNL950 by reduction of the shear of the mean flow and reduction in the streak amplitude (cf. Fig. 3).

A comparison of the perturbation statistics of RNL950 with NS950 is shown in Fig. 4. The u' component of the perturbation velocity fluctuations are significantly more pronounced in RNL950 (cf. Fig. 4a) and the magnitude of the streak in RNL950 exceeds significantly the streak magnitude in NS950 in the inner wall region (cf. Fig. 4b). In contrast, the wall-normal and spanwise fluctuations in RNL950 are less pronounced than in NS950 (cf. Fig. 4c,d) and the streak fluctuations in the outer region are also less pronounced in RNL950 (cf. Fig. 4b).

Despite these differences in the r.m.s. values of the velocity fluctuations, both RNL950 and NS950 produce very similar uv Reynolds stress (cf. Fig. 5). The Reynolds stress $-[uv]_{x,z,t}$ is the sum of $-[U_sV]_{z,t}$ and $-[u'v']_{x,z,t}$. Comparison of the wall-normal
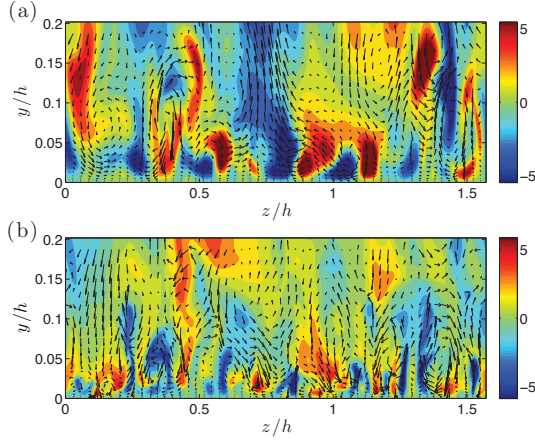
Figure 6: Perturbation structure, $\mathbf{u}'^{+}$ in (y,z) plane cross-section for (a) RNL950 and (b) NS950 in the inner wall region, $0 \leqslant y/h \leqslant 0.2$. Both panels show contours of the u'^{+} field, superimposed with components the (v'^{+}, w'^{+}) velocities.
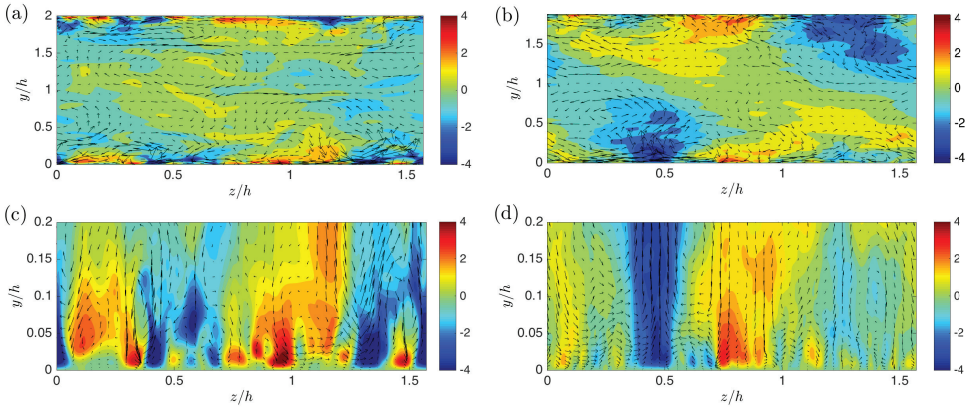

Figure 7: Instantaneous streak component of the flow, U_s^{+}, shown as a (y,z) plane cross-section for (a), (c) RNL950 and (b), (d) NS950. All panels show contours of the streak velocity, U_s^{+}, superimposed with the components of the (V^{+}, W^{+}) velocities. The top panels show the whole channel while the bottom panels show the inner wall region, $0 \leqslant y/h \leqslant 0.2$.

distribution of the time mean of these two components of the Reynolds stress is shown in Fig. 5a. Because the turbulence in NS950 and RNL950 is sustained with essentially the same pressure gradient, the sum of these Reynolds stresses is the same linear function of y outside the viscous layer in these simulations. The Reynolds stress is dominated by the perturbation Reynolds stress $-[u'v']_{x,z,t}$ in all simulations, with the RNL stress penetrating farther from the wall. This is consistent with the fact that the perturbation structure in RNL has larger scale. This can be seen in a comparison of the NS and RNL perturbation structure shown in Fig. 6. Note that the Reynolds stress $-[U_s V]_{z,t}$ associated with the streak and roll in the outer region of the NS950 simulation is larger than that in RNL950. Further, the average correlation between the perturbation u' and
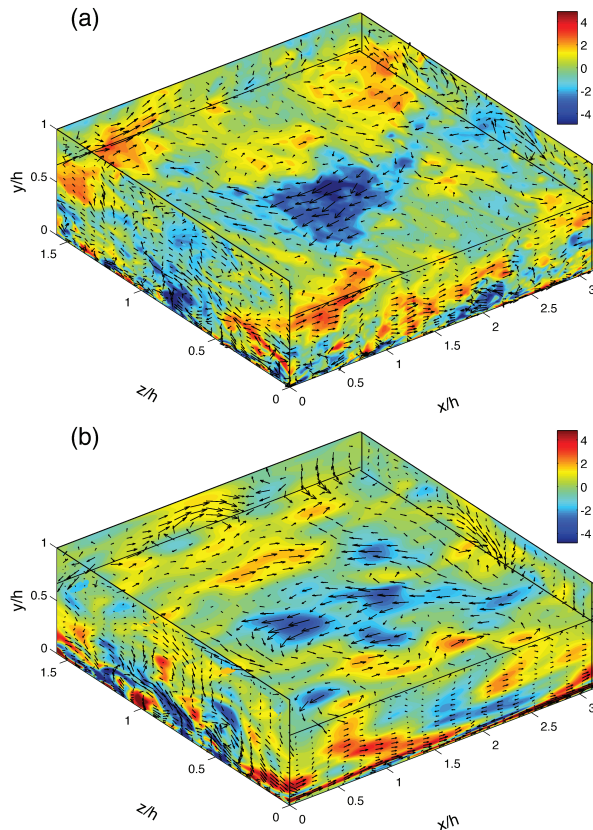
Figure 8: 3D perspective plots of the flow at a single time for (a) NS950, and (b) RNL950 for lower half of the channel, $0 \leqslant y/h \leqslant 1$. Both images show contours of the streak component plus streamwise perturbation, $U_s^+ + u'^+$. The central x-z panel shows the flow at channel height, $y/h = 0.65$. The superimposed vectors represent the $(U_s^+ + u'^+, w^+)$ velocities for the (x, z)-plane, $(U_s^+ + u'^+, v^+)$ velocities for the (x, y)-plane and (v^+, w^+) velocities for the (y, z)-plane. The parameters of the simulations are given in table 1.

v' fields are almost the same in both simulations while the correlation between the U_s and V in RNL950 is much smaller than that in NS950 in the outer layer. This is seen in a plot of the structure coefficient (cf. Flores & Jiménez (2006)) shown in Fig. 5b.

Turning now to the flow structures in the NS950 and RNL950 simulations, a (y, z) plane snapshot of the streamwise mean flow component (corresponding to $k_x = 0$ streamwise wavenumber) is shown in Fig. 7. Contours of the streamwise streak, U_s, are shown together with vectors of the streamwise mean (V, W) field, which indicates the velocity components of the large-scale roll structure. The presence of organized streaks and associated rolls is evident both in the inner-wall and in the outer-wall region. Note that in comparison with the streak in NS950, the streak in RNL950 has a finer (y, z) structure which is consistent with the energy of the streak being more strongly dissipated by diffusion in RNL (cf. Fig. 7). A three-dimensional perspective of the flow in NS950 and RNL950 is shown in Figure 8. Note that in RNL950 there is no visual evidence of the $k_x = 0$ roll/streak structure which is required by the restriction of RNL dynamics to be the primary structure responsible for organizing and maintaining the self-sustained turbulent state. Rather, the most energetic structure among the perturbations maintaining the pivotal streamwise

mean roll/streak is the structure that dominates the observed turbulent state. We interpret this as indicating that the $k_x = 0$ roll/streak structure, which is the dynamically central organizing structure in RNL turbulence and which organizes the turbulence on scale unbounded in the streamwise direction, cannot be reliably identified by visual inspection of the flow fields which would lead one to conclude that the organizing scale was not just finite but the rather short scale of the separation between perturbations to the streak. Essentially this same argument is cast in terms of the inability of Fourier analysis to identify the organization scale of the roll/streak structure by Hutchins & Marusic (2007). This dynamically central structure which appears necessarily at $k_x = 0$ in RNL dynamics is reflected in the highly streamwise elongated structures seen in simulations and observations of DNS wall turbulence. In the short channel used here the $k_x = 0$ component is prominent in both the RNL950 and DNS950 (cf. Fig. 7).

An alternative view of turbulence structure is provided by comparison of the spectral energy densities of velocity fields as a function of streamwise and spanwise wavenumber, (k_x, k_z). The premultiplied spectral energy densities of each of the three components of velocity, E_{uu}, E_{vv} and E_{ww}, are shown at heights $y^+ = 20$, representative of the inner-wall region; and at $y/h = 0.65$, representative of the outer-wall region, in Fig. 9. While RNL950 produces spanwise streak spacing and rolls similar to those in NS950, the tendency of RNL to produce longer structures in this diagnostic is also evident. The spectra for the outer region indicate similar large-scale structure and good agreement in the spanwise spacing between RNL950 and NS950. This figure establishes the presence of large-scale structure in the outer region in both RNL950 and NS950. It has been noted that in NS950 while the dominant large-scale structures scale linearly with distance from the wall in the inner-wall region, in the outer regions structures having the largest possible streamwise scale dominate the flow variance at high Reynolds number (Jiménez 1998; Jiménez & Hoyas 2008). This linear scaling near the wall can also be seen in Fig. 10 where contour plots of normalized premultiplied one-dimensional spectral energy densities as a function of spanwise wavelength, k_z, and wall-normal distance, as in Jiménez (1998); Jiménez & Hoyas (2008), for both NS950 and RNL950. In both simulations the spanwise wavelength associated with the spectral density maxima increases linearly with wall distance and this linear dependence is intercepted at $y/h \approx 0.5$ (or $y^+ \approx 450$). Beyond $y/h \approx 0.5$ structures assume the widest wavelength allowed in the channel, suggesting simulations be performed in larger boxes in future work (cf. discussion by Jiménez & Hoyas (2008) and Flores & Jiménez (2010)). Corresponding contour plots of spectral energy density as a function of streamwise wavelength and wall-normal distance are shown in Fig. 11. These plots show that the perturbation variance in the inner wall and outer wall region is concentrated in a limited set of streamwise components which is also apparent in Fig. 8. The spontaneous restriction on streamwise perturbation wavenumber support that occurs in RNL dynamics produces a corresponding sharp shortwave cutoff in the k_x components of the RNL950 simulation spectra as seen in panels (d,e,f) of Fig. 11. Note that the maximum wavelength in these graphs is equal to the streamwise length of the box and not to the infinite wavelength associated with the energy of the roll/streak structure in RNL dynamics.

6. Streak structure dynamics in NS and RNL dynamics

That RNL dynamics maintains a turbulent state similar to that of NS with nearly the same Re_τ ($Re_\tau = 882$ with the 6 Fourier components of RNL950 and $Re_\tau = 970.2$ for the single Fourier component with $k_x h = 12$ of RNL950k_x12 vs. $Re_\tau = 940$ of the NS950; cf. table 1) implies that these systems have approximately the same energy production
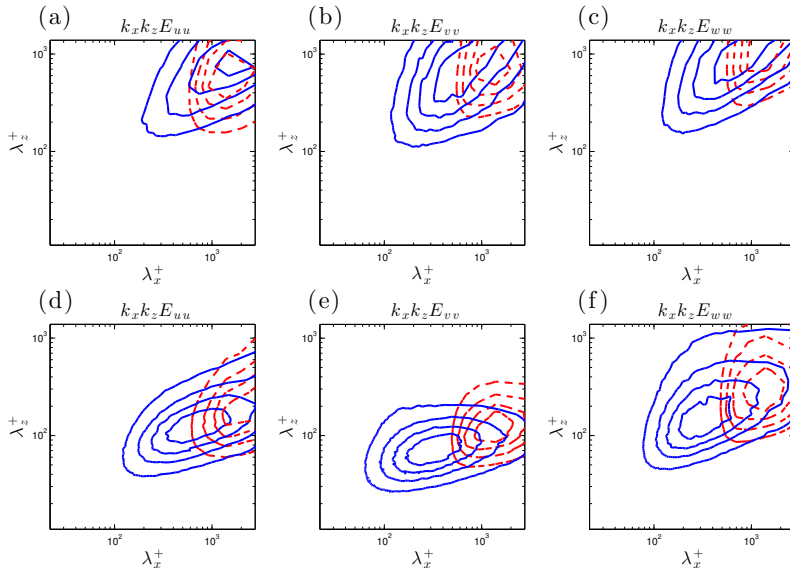
Figure 9: Contours of pre-multiplied power spectra $k_x k_z E_{ff}(k_x, k_z)$ with $f = u, v, w$, as a function of λ_x^+ and λ_z^+ for NS950 (solid) and RNL950 (dashed). Panels (a), (b) and (c) show the spectral energy densities at wall distance $y/h = 0.65$ for the u, v and w respectively, while panels (d), (e) and (f) show the corresponding spectral energy densities at $y^+ = 20$. Contours are (0.2,0.4,0.6,0.8) times the maximum value of the corresponding spectrum. The maximum λ_x^+ and λ_y^+ are the lengths L_x^+, L_z^+ of the periodic channel.

and dissipation and that the reduced set of Fourier components retained in RNL dynamics assume the burden of accounting for this energy production and dissipation. Specifically, the components in NS950 that are not retained in RNL dynamics are responsible for approximately 1/3 of the total energy dissipation, which implies that the components that are retained in RNL950 dynamics must increase their dissipation, and consistently their amplitude, by that much.

Large scale roll/streak structures are prominent in the inner layer as well as in the outer layer both in NS950 and in RNL950. The dynamics of this structure can be diagnosed using the time evolution of the energy of each k_x component during the transition from NS to RNL, shown in Fig. 2b. It can be seen in the short NS950 box that the energy associated with the streamwise mean structure with $k_x = 0$ and $k_z \neq 0$ is dominant among the structures that deviate from the mean flow, $[U]_{z,t}$. In the inner layer the interaction of roll/streak structures with the $k_x \neq 0$ perturbation field maintains turbulence through an SSP (Hamilton *et al.* 1995; Jiménez & Pinelli 1999; Farrell & Ioannou 2012). The RNL system provides an especially simple manifestation of this SSP as its dynamics comprise only interaction between the mean ($k_x = 0$) and perturbation ($k_x \neq 0$) components. The fact that RNL self-sustains a close counterpart of the DNS turbulent state in the inner wall region provides strong evidence that the RNL SSP captures the essential dynamics of turbulence in this region.

The structure of the RNL system compels the interpretation that the time dependence of the SSP cycle in this system, which might appear to an observer to consist of a concatenation of random and essentially unrelated events, is instead an intricate interaction dynamics among streaks, rolls and perturbations that produces the time dependent
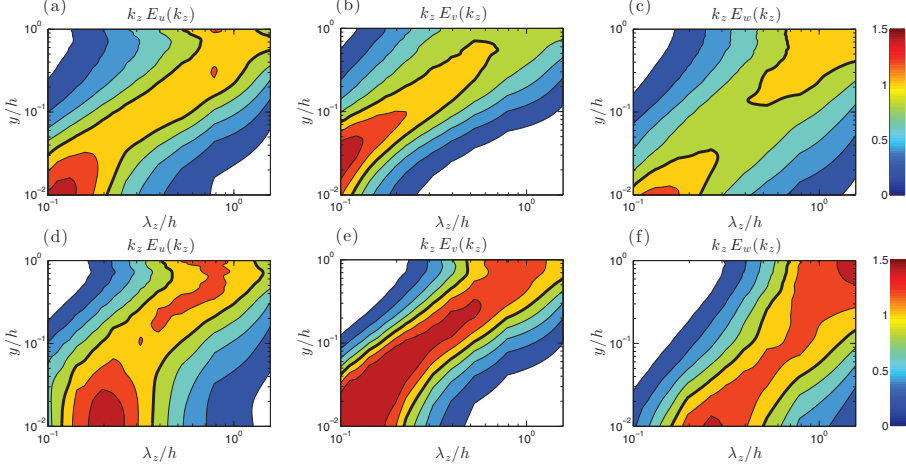
Figure 10: Normalized pre-multiplied spectral densities $k_z E_f(k_z) = k_z \sum_{k_x} E_{ff}(k_x, k_z)$, with $f = u, v, w$, as a function of spanwise wavelength, λ_z/h, and y/h. Spectral densities are normalized so that at each y the total energy, $\sum_{k_z} E_f(k_z)$, is the same. Shown are for NS950 (a): $k_z E_u(k_z)$, (b): $k_z E_v(k_z)$, (c): $k_z E_w(k_z)$ and for RNL950 (d): $k_z E_u(k_z)$, (e): $k_z E_v(k_z)$, (f): $k_z E_w(k_z)$. The isocontours are $0.2, 0.4, \ldots, 1.4$ and the thick line marks the 1.0 isocontour.
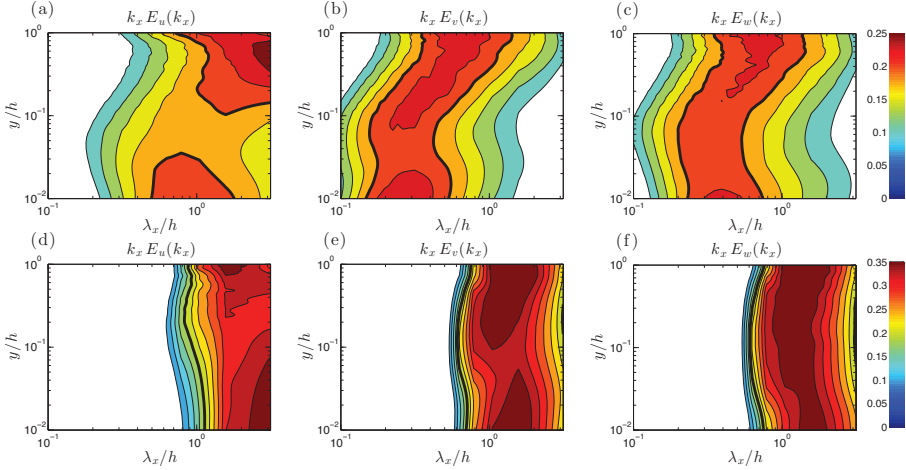

Figure 11: Normalized pre-multiplied spectral densities $k_x E_f(k_x) = k_x \sum_{k_z} E_{ff}(k_x, k_z)$, with $f = u, v, w$, as a function of streamwise wavelength, λ_x/h, and y/h. Spectral densities are normalized so that at each y the total energy, $\sum_{k_x} E_f(k_x)$, is the same. Shown are for NS950 (a): $k_x E_u(k_x)$, (b): $k_x E_v(k_x)$, (c): $k_x E_w(k_x)$ and for RNL950 (d): $k_x E_u(k_x)$, (e): $k_x E_v(k_x)$, (f): $k_x E_w(k_x)$. The isocontours are $0.1, 0.125, \ldots, 0.35$ and the thick line marks the 0.2 isocontour.
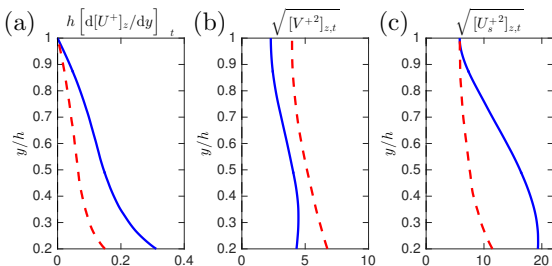
Figure 12: Comparison of the turbulent mean shear, $[\mathrm{d}[U^+]_z/\mathrm{d}y]_t\, h$ (panel (a)), the r.m.s. of $[V^+]_z$ (panel (b)) and the r.m.s. of the streak velocity, U_s^+, (panel (c)) for NS950 (solid) and RNL950 (dashed) in the outer layer, $0.2 \leqslant y/h \leqslant 1$.

streamwise mean flow $\mathbf{U}(y, z, t)$ which, when introduced in (2.7b), results in generation of a particular evolving perturbation Lyapunov structure with exactly zero Lyapunov exponent that simultaneously produces Reynolds stresses contrived to maintain the associated time dependent mean flow. S3T identifies this exquisitely contrived SSP cycle comprising the generation of the streak through lift-up by the rolls, the maintenance of the rolls by torques induced by the perturbations which themselves are maintained by time-dependent parametric non-normal interaction with the streak (Farrell & Ioannou 2012).

This statistical equilibrium SSP cycle is more efficient than its DNS counterpart in producing downgradient perturbation momentum flux as with smaller mean shear over most of the channel a self-sustained turbulence with approximately the same Re_τ as that in NS950 is maintained, as discussed above (cf. section 5). A comparison of the shear, of the r.m.s. V velocity, and of the r.m.s. streak velocity, U_s, in the outer layer is shown as a function of y in Fig. 12, from which it can be seen that the fractional reduction of the amplitude of the streak in the transition to RNL is approximately equal to the fractional reduction in the mean flow shear. It is important to note that these dependencies arise due to the feedback control exerted by the perturbation dynamics on the mean flow dynamics in the RNL system by which its statistical steady state is determined. The structure of RNL isolates this feedback control process so that it can be studied and elucidating its mechanism and properties are the subject of ongoing work.

In the discussion above we have assumed that the presence of roll and streak structure in the log-layer in RNL indicates the existence of an SSP cycle there and by implication also in NS. In order to examine this SSP consider the momentum equation for the streamwise streak:

$$\partial_t U_s = \underbrace{-\left(V\,\partial_y U - [V\,\partial_y U]_z\right) - \left(W\,\partial_z U - [W\,\partial_z U]_z\right)}_{A}$$

$$\underbrace{-\left(\left[v'\,\partial_y u' - [v'\,\partial_y u']_z\right]_x\right) - \left(\left[w'\,\partial_z u' - [w'\,\partial_z u']_z\right]_x\right)}_{B} + \underbrace{\nu\,\Delta U_s}_{C} \ . \quad (6.1)$$

Term A in (6.1) is the contribution to the streak acceleration by the 'lift-up' mechanism and the 'push-over' mechanism, which represent transfer to streak momentum by the mean wall-normal and spanwise velocities respectively; Term B in (6.1) is the contribution to the streak momentum by the perturbation Reynolds stress divergence (structures with $k_x \neq 0$); Term C is the diffusion of the streak momentum due to viscosity.

In order to identify the mechanism of streak maintenance we determine the contribution of terms A, B and C in (6.1) to the streak momentum budget by evaluating these contributions. The time averaged results are shown as a function of y over these cross-stream regions of the flow, indicated by R: the whole channel, the outer region, $0.2 \leqslant$
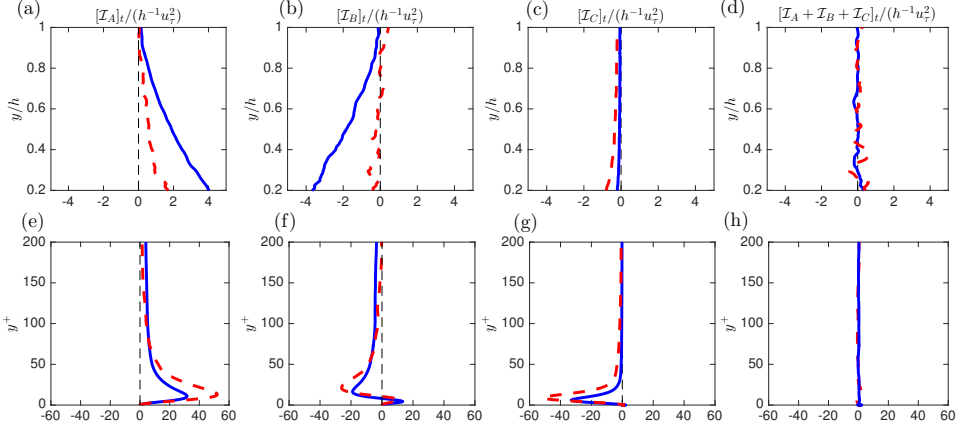
Figure 13: Cross-stream structure of the time averaged contributions to streak acceleration for NS950 (solid) and RNL950 (dashed) from: (a,e) the lift-up mechanism $[\mathcal{I}_A]_t(y)$, (b,f) the perturbation Reynolds stress divergence $[\mathcal{I}_B]_t(y)$ and (c,g) the momentum diffusion $[\mathcal{I}_C]_t(y)$. Upper panels show structure in the outer layer, $0.2 \leqslant y/h \leqslant 1$, lower panels show the structure in the inner layer, $0 \leqslant y^+ \leqslant 200$. In (d,h) we plot the sum of these terms which averaged over a long time interval should add exactly to zero.
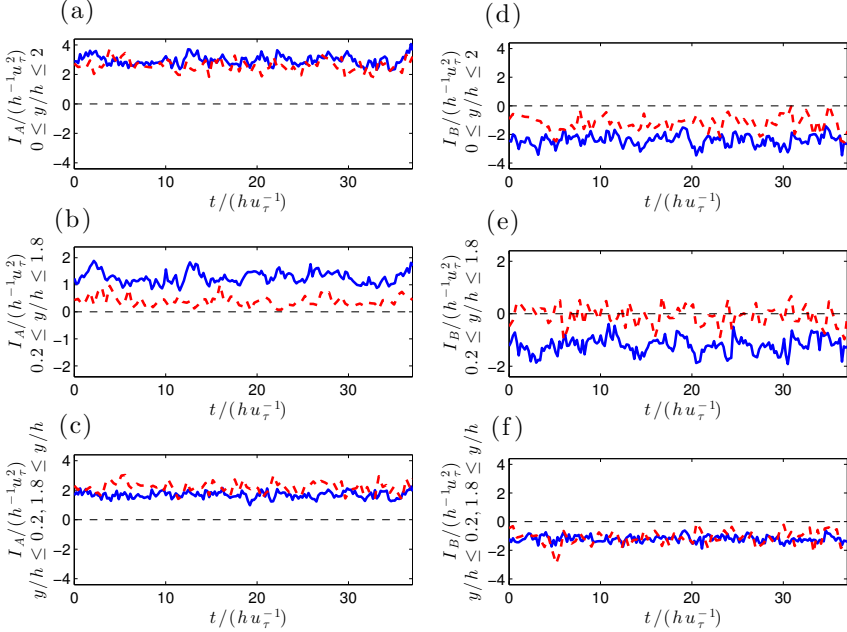

Figure 14: Time series of the total $I_A(t)$ (lift-up) for NS950 (solid) and RNL950 (dashed), (a): over the whole channel, (b): over the outer region, $0.2 \leqslant y/h \leqslant 1.8$, (c): over the inner region, $0 \leqslant y/h \leqslant 0.2$ and $1.8 \leqslant y/h \leqslant 2$. Similarly for $I_B(t)$ (Reynolds stress divergence), (d): over the whole channel, (e): over the outer region, $0.2 \leqslant y/h \leqslant 1.8$, (f): over the inner region, $0 \leqslant y/h \leqslant 0.2$ and $1.8 \leqslant y/h \leqslant 2$.

$y/h \leqslant 1.8$ and the inner region, $0 \leqslant y/h < 0.2$ and $1.8 < y/h \leqslant 2$, in Fig 13. The contributions are respectively the lift up:

$$I_A(t) = h^{-1} \int_R \mathrm{d}y \; \mathcal{I}_A(y,t) \;, \quad \text{with} \;\; \mathcal{I}_A(y,t) = \Big[\mathrm{sgn}(U_s) \times (\text{Term A}) \Big]_z \;, \qquad (6.2)$$

the perturbation Reynolds stress divergence,

$$I_B(t) = h^{-1} \int_R \mathrm{d}y \; \mathcal{I}_B(y,t) \;, \quad \text{with} \;\; \mathcal{I}_B(y,t) = \Big[\mathrm{sgn}(U_s) \times (\text{Term B}) \Big]_z \;, \qquad (6.3)$$

and diffusion,

$$I_C(t) = h^{-1} \int_R \mathrm{d}y \; \mathcal{I}_C(y,t) \;, \quad \text{with} \;\; \mathcal{I}_C(y,t) = \Big[\mathrm{sgn}(U_s) \times (\text{Term C}) \Big]_z \;, \qquad (6.4)$$

In the inner and outer wall regions in both NS950 and RNL950 the streak is maintained only by the lift-up mechanism, while streak momentum is lost on average at all cross-stream levels to both the Reynolds stress divergence and the momentum diffusion. In RNL950 the magnitude of streak acceleration by lift-up is greater than that of NS950 in the inner region, in the outer region the acceleration by lift-up in RNL950 is about half that in NS950 consistent with their similar roll amplitude (cf. Fig. 12b) but the smaller mean flow shear maintained at statistical steady state in RNL950. In the outer region of the NS950 the Reynolds stress divergence almost completely balances the positive contribution from lift-up while in RNL950 the lift up is balanced equally by the Reynolds stress divergence and the diffusion. Enhancement of the contribution by diffusion in the outer layer in RNL950 results from the increase in the spanwise and cross-stream wavenumbers of the streak (cf. Fig. 7c) resulting from the nonlinear advection of the streak by the V and W velocities. This increase in the spanwise and cross-stream wavenumbers of the streak in RNL950 due to nonlinear advection by the mean (V, W) roll circulation also implies that the dissipation of streak energy in RNL950 is similarly enhanced. This constitutes an alternative route for energy transfer to the dissipation scale which continues to be available for establishment of statistical equilibrium in RNL950 despite the limitation in the streamwise wavenumber support inherent in RNL turbulence. The lift-up process is a positive contribution to the maintenance of the streak and the Reynolds stress divergence is a negative contribution not only in a time averaged sense but also at every time instant. This is shown in plots of the time series of the lift up and Reynolds stress divergence contribution to the streak momentum over the inner region $0 \leqslant y/h < 0.2$ and $1.8 < y/h \leqslant 2$, over the outer region $0.2 \leqslant y/h \leqslant 1.8$ and over the whole channel in Fig. 14. We conclude that in both NS950 and RNL950 the sole positive contribution to the outer layer streaks is lift-up, despite the small shear in this region. We next consider the dynamics maintaining the lift-up.

7. Roll dynamics: maintenance of mean streamwise vorticity in NS and RNL

We have established that the lift-up mechanism is not only responsible for streak maintenance in the inner layer but also in the outer layer. We now examine the mechanism of the lift-up by relating it to maintenance of the roll structure using as a diagnostic streamwise averaged vorticity, $\Omega_x = \partial_y W - \partial_z V$. In order for roll circulation to be maintained against dissipation there must be a continuous generation of Ω_x. There are two possibilities for the maintenance of Ω_x in the outer layer: either Ω_x is generated locally in the outer layer, or it is advected from the near wall region.
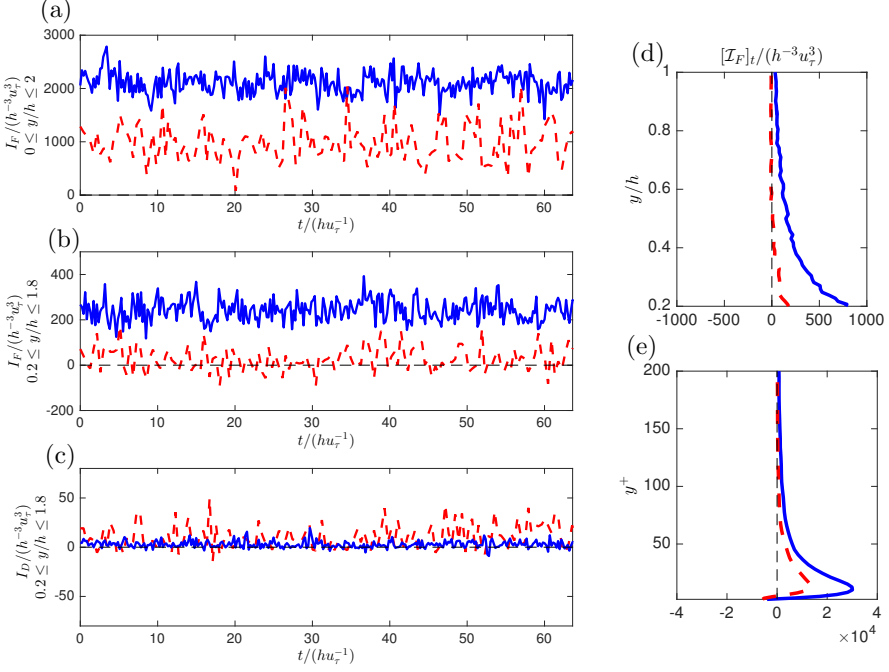
Figure 15: (a)-(c) Time series of the contribution to the time rate of change of streamwise square vorticity $\int dy \left[\Omega_x^2/2\right]_z$ by perturbation torques, I_F, and by advection of streamwise mean vorticity by the mean flow, I_D, for NS950 (solid) and RNL950 (dashed). (a) I_F over the whole channel, $0 \leqslant y/h \leqslant 2$ ($I_D = 0$ in this case). The time mean I_F is $2103.6 \, h^{-3} u_\tau^3$ for NS950 and $982.8 \, u_\tau^3$ for RNL950. (b) I_F over the outer layer, $0.2 \leqslant y/h \leqslant 1.8$. The time mean I_F for this region is $242.5 \, h^{-3} u_\tau^3$ for NS950 and only $28.7 \, h^{-3} u_\tau^3$ for RNL950. (c) I_D for the outer layer $0.2 \leqslant y/h \leqslant 1.8$. The time mean I_D is $2.9 \, h^{-3} u_\tau^3$ for NS950 and $11.2 \, h^{-3} u_\tau^3$ for RNL950. These figures show that in NS950 and RNL950 the roll is maintained locally by the perturbation Reynolds stresses. (d,e) Cross-stream structure of the time averaged contribution to the streamwise mean vorticity generation from perturbation Reynolds stress induced torques $[\mathcal{I}_F]_t(y)$.

From (2.1a) we have that Ω_x satisfies the equation:

$$\partial_t \Omega_x = \underbrace{- \left(V \, \partial_y + W \, \partial_z\right) \Omega_x}_{D} + \underbrace{\left(\partial_{zz} - \partial_{yy}\right) \left[v'w'\right]_x - \partial_{yz} \left(\left[w'^2\right]_x - \left[v'^2\right]_x\right)}_{F} + \nu \, \Delta \Omega_x \; .$$

(7.1)

Term D expresses the streamwise vorticity tendency due to advection of Ω_x by the streamwise mean flow (V, W). Because there is no vortex stretching contribution to Ω_x from the (V, W) velocity field, this term only advects the Ω_x field and cannot sustain it against dissipation. However, this term may be responsible for systematic advection of Ω_x from the inner to the outer layer. Term F is the torque induced by the perturbation field. This is the only term that can maintain Ω_x. The overall budget for square streamwise

vorticity in the region R, $y_1 \leqslant y \leqslant y_2$, $0 \leqslant z \leqslant L_z$, is given by:

$$\partial_t \int\limits_{y_1}^{y_2} \mathrm{d}y \frac{1}{2} \left[\Omega_x^2 \right]_z = \underbrace{-\frac{1}{2} \left[\Omega_x^2 V \right]_z \Big|_{y=y_1}^{y_2}}_{=h\,I_D} + \underbrace{\int\limits_{y_1}^{y_2} \mathrm{d}y \left[\Omega_x \times \text{Term F} \right]_z}_{=h\,I_F} + \nu \int\limits_{y_1}^{y_2} \mathrm{d}y \left[\Omega_x\,\Delta\Omega_x \right]_z ,$$

$$(7.2)$$

where:

$$I_D(t) = h^{-1} \int_R \mathrm{d}y\, \mathcal{I}_D(y,t)\ , \text{with}\ \ \mathcal{I}_D(y,t) = \left[\Omega_x \times (\text{Term D}) \right]_z , \qquad (7.3)$$

to be the advection into cross-stream region, R, and

$$I_F(t) = h^{-1} \int_R \mathrm{d}y\, \mathcal{I}_F(y,t)\ , \text{with}\ \ \mathcal{I}_D(y,t) = \left[\Omega_x \times (\text{Term D}) \right]_z , \qquad (7.4)$$

the Reynolds stress torque production in region R.

Time series of the contributions from $I_D(t)$ and $I_F(t)$ to the Ω_x production for NS950 and RNL950, shown in Fig. 15, demonstrate that Ω_x is primarily generated in situ by Reynolds stress torques. The corresponding wall-normal structure of the time mean of $\mathcal{I}_F$, representing the local contribution to streamwise mean vorticity generation from perturbation Reynolds stress induced torques is shown in Fig. 15d,e. Note that for NS950 in the outer layer the streamwise mean vorticity generation by the Reynolds stress is strongly positive at each instant. This implies a systematic positive correlation between the roll circulation and the torque from Reynolds stress with the torque configured so as to maintain the roll. S3T theory explains this systematic correlation between the roll/streak structure and the perturbation torques maintaining it as a direct consequence of the straining of the perturbation field by the streak (Farrell & Ioannou 2012).

Having established that the streamwise vorticity in the outer layer is maintained in situ by systematic correlation of Reynolds stress torque with the roll circulation we conclude that the SSP cycle in both NS and RNL operates in the outer layer in a manner essentially similar to that in the inner layer.

8. Discussion and Conclusions

We have established that RNL self-sustains turbulence at moderate Reynolds numbers in pressure driven channel flow, despite its greatly simplified dynamics when compared to NS. Remarkably, in the RNL system, the turbulent state is maintained by a small set of structures with low streamwise wavenumber Fourier components (at $Re_\tau = 950$ with the chosen channel the SSP involves only the $k_x = 0$ streamwise mean and the next 6 streamwise Fourier components). Not only that, but this minimal turbulent dynamics arises spontaneously when the RNL system is initialized by NS turbulence at the same Reynolds number. In this way RNL spontaneously produces a turbulent state of reduced complexity. RNL identifies an exquisitely contrived SSP cycle which has been previously identified to comprise the generation of the streak through lift-up by the rolls, the maintenance of the rolls by torques induced by the perturbations which themselves are maintained by an essentially time-dependent parametric non-normal interaction with the streak (rather than e.g. inflectional instability of the streak structure) (Farrell & Ioannou 2012). The vanishing of the Lyapunov exponent associated with the SSP is indicative of a feedback control process acting between the streaks and the perturbations by which the parametric instability that sustains the perturbations on the time dependent streak is reduced to zero Lyapunov exponent, so that the turbulence neither diverges nor decays.

We have established that both NS and RNL produce a roll/streak structure in the outer layer and that an SSP is operating there despite the low shear in this region. It has been shown elsewhere that turbulence self-sustains in the log-layer in the absence of boundaries (Mizuno & Jiménez 2013). This is consistent with our finding that an SSP cycle exists in both the inner-layer and outer-layer.

The turbulence maintained in RNL is closely related to its associated NS turbulence and both exhibit a log-layer, although with substantially different von Kármán constants for some RNL truncations in streamwise wavenumber. Existence of a log-layer is a fundamental requirement of asymptotic matching between regions with different spatial scaling, as was noted by Millikan (1938). However, the exact value of the von Kármán constant does not have a similar fundamental basis in analysis and RNL turbulence, which is closely related to NS turbulence but more efficient in producing Reynolds stress, maintains as a consequence a smaller shear and therefore greater von Kármán constant. Specifically, we have determined that the SSP cycle in RNL is characterized by a more energetic and larger scale perturbation structure, despite having a lower amplitude streak and mean shear.

Formation of roll/streak structures in the log-layer is consistent with the universal mechanism by which turbulence is modified by the presence of a streak in such way as to induce growth of a roll structure configured to lead to continued growth of the original streak. This growth process underlies the non-normal parametric mechanism maintaining perturbation variance in the SSP that maintains turbulence (Farrell & Ioannou 2012). This universal mechanism does not predict nor require that the roll/streak structures be of finite streamwise extent and in its simplest form it has been demonstrated that it supports roll/streak structures with zero streamwise wavenumber. From this point of view the observed length of roll/streak structures is not a consequence of the primary mechanism of the SSP supporting them but rather a secondary effect of disruption by the turbulence. In this work we have provided evidence that NS turbulence is closely related in its dynamics to RNL turbulence from the wall through the log-layer. Moreover, given that the dynamics of RNL turbulence can be understood fundamentally from its direct relation with S3T turbulence we conclude that the mechanism of turbulence in wall bounded shear flow can be insightfully related to the analytically tractable roll/streak/perturbation SSP that was previously identified to maintain S3T turbulence. We conclude that the severe restriction of the dynamics coupled with the restricted support of the dynamics in streamwise wavenumber that are inherent in the RNL system result in the establishment of a statistically steady turbulent state in which, while the maintained statistics differ in particulars from those of a DNS at the same *Re*, these systems share fundamental aspects of both structure and dynamics and that this relation provides an attractive pathway to further understanding of wall-turbulence.

REFERENCES

DEL ÁLAMO, J. C., JIMÉNEZ, J., ZANDONADE, P. & MOSER, R. D. 2004 Scaling of the energy spectra of turbulent channels. *J. Fluid Mech.* **500**, 135–144.

DEL ÁLAMO, J. C., JIMÉNEZ, J., ZANDONADE, P. & MOSER, R. D. 2006 Self-similar vortex clusters in the turbulent logarithmic region. *J. Fluid Mech.* **561**, 329–358.

Bakas, N. A. & Ioannou, P. J. 2013 Emergence of large scale structure in barotropic β-plane turbulence. *Phys. Rev. Lett.* **110**, 224501.

Bullock, K. J., Cooper, R. E. & Abernathy, F. H. 1978 Structural similarity in radial correlations and spectra of longitudinal velocity fluctuations in pipe flow. *J. Fluid Mech.* **88**, 585–608.

Constantinou, N. C., Farrell, B. F. & Ioannou, P. J. 2014a Emergence and equilibration of jets in beta-plane turbulence: applications of Stochastic Structural Stability Theory. *J. Atmos. Sci.* **71** (5), 1818–1842.

Constantinou, N. C., Farrell, B. F. & Ioannou, P. J. 2015 Statistical state dynamics of jet/wave coexistence in beta-plane turbulence. *J. Atmos. Sci.* (sub judice, arXiv:1509.06326).

Constantinou, N. C., Lozano-Durán, A., Nikolaidis, M.-A., Farrell, B. F., Ioannou, P. J. & Jiménez, J. 2014b Turbulence in the highly restricted dynamics of a closure at second order: comparison with DNS. *J. Phys. Conf. Ser.* **506**, 012004.

Dallas, V., Vassilicos, J. C. & Hewitt, G. F. 2009 Stagnation point von Kármán coefficient. *Phys. Rev. E* **80**, 046306.

Farrell, B. F., Gayme, D. F., Ioannou, P. J., Lieu, B. K. & Jovanović, M. R. 2012 Dynamics of the roll and streak structure in transition and turbulence. *CTR, Proceedings of the Summer Program* pp. 43–54.

Farrell, B. F. & Ioannou, P. J. 1996 Generalized stability. Part II: Non-autonomous operators. *J. Atmos. Sci.* **53**, 2041–2053.

Farrell, B. F. & Ioannou, P. J. 2003 Structural stability of turbulent jets. *J. Atmos. Sci.* **60**, 2101–2118.

Farrell, B. F. & Ioannou, P. J. 2007 Structure and spacing of jets in barotropic turbulence. *J. Atmos. Sci.* **64**, 3652–3665.

Farrell, B. F. & Ioannou, P. J. 2008 Formation of jets by baroclinic turbulence. *J. Atmos. Sci.* **65**, 3353–3375.

Farrell, B. F. & Ioannou, P. J. 2009a Emergence of jets from turbulence in the shallow-water equations on an equatorial beta plane. *J. Atmos. Sci.* **66**, 3197–3207.

Farrell, B. F. & Ioannou, P. J. 2009b A stochastic structural stability theory model of the drift wave-zonal flow system. *Phys. Plasmas* **16**, 112903.

Farrell, B. F. & Ioannou, P. J. 2012 Dynamics of streamwise rolls and streaks in turbulent wall-bounded shear flow. *J. Fluid Mech.* **708**, 149–196.

Flores, O. & Jiménez, J. 2006 Effect of wall-boundary disturbances on turbulent channel flows. *J. Fluid Mech.* **566**, 357–376.

Flores, O. & Jiménez, J. 2010 Hierarchy of minimal flow units in the logarithmic layer. *Phys. Fluids* **22**, 071704.

Foias, C., Manley, O., Rosa, R. & Temam, R. 2001 *Navier-Stokes Equations and Turbulence*. Cambridge University Press, Cambridge.

Gayme, D. F. 2010 A robust control approach to understanding nonlinear mechanisms in shear flow turbulence. PhD thesis, Caltech, Pasadena, CA, USA.

Gayme, D. F., McKeon, B. J., Papachristodoulou, A., Bamieh, B. & Doyle, J. C. 2010 A streamwise constant model of turbulence in plane Couette flow. *J. Fluid Mech.* **665**, 99–119.

Hamilton, K., Kim, J. & Waleffe, F. 1995 Regeneration mechanisms of near-wall turbulence structures. *J. Fluid Mech.* **287**, 317–348.

Hellström, Leo H. O., Sinha, A. & Smits, A. J. 2011 Visualizing the very-large-scale motions in turbulent pipe flow. *Phys. Fluids* **23**, 011703.

Hutchins, N. & Marusic, I. 2007 Evidence of very long meandering features in the logarithmic region of turbulent boundary layers. *J. Fluid Mech.* **579**, 1–28.

Jiménez, J. 1998 The largest scales of turbulent wall flows. *CTR Annual Research Briefs* pp. 137–154.

Jiménez, J. & Hoyas, S. 2008 Turbulent fluctuations above the buffer layer of wall-bounded flows. *J. Fluid Mech.* **611**, 215–236.

Jiménez, J. & Pinelli, A. 1999 The autonomous cycle of near-wall turbulence. *J. Fluid Mech.* **389**, 335–359.

KIM, J., MOIN, P. & MOSER, R. 1987 Turbulence statistics in fully developed channel flow at low Reynolds number. *J. Fluid Mech.* **177**, 133–166.

KIM, K.C. & ADRIAN, R. J. 1999 Very large-scale motion in the outer layer. *Phys. Fluids* **11**, 417–422.

KLINE, S. J., REYNOLDS, W. C., SCHRAUB, F. A. & RUNSTADLER, P. W. 1967 The structure of turbulent boundary layers. *J. Fluid Mech.* **30**, 741–773.

LOZANO-DURÁN, A., FLORES, O. & JIMÉNEZ, J. 2012 The three-dimensional structure of momentum transfer in turbulent channels. *J. Fluid Mech.* **694**, 100–130.

LOZANO-DURÁN, A. & JIMÉNEZ, J. 2014a Effect of the computational domain on direct simulations of turbulent channels up to $Re_\tau = 4200$. *Phys. Fluids* **26**, 011702.

LOZANO-DURÁN, A. & JIMÉNEZ, J. 2014b Time-resolved evolution of coherent structures in turbulent channels: characterization of eddies and cascades. *J. Fluid Mech.* **759**, 432–471.

MARSTON, J. B., CONOVER, E. & SCHNEIDER, T. 2008 Statistics of an unstable barotropic jet from a cumulant expansion. *J. Atmos. Sci.* **65** (6), 1955–1966.

MARUSIC, I., MCKEON, B. J., MONKEWITZ, P.A., NAGIB, H. M. & SREENIVASAN, K. R. 2010 Wall-bounded turbulent flows at high Reynolds numbers: Recent advances and key issues. *Phys. Fluids* **22**, 065103.

MILLIKAN, C. B. 1938 A critical discussion of turbulent flows in channels and circular tubes. In *Proceedings of the Fifth International Congress for Applied Mechanics*. Wiley, New York.

MIZUNO, Y. & JIMÉNEZ, J. 2013 Wall turbulence without walls. *J. Fluid Mech.* **723**, 429–255.

PARKER, J. B. & KROMMES, J. A. 2014 Generation of zonal flows through symmetry breaking of statistical homogeneity. *New J. Phys.* **16** (3), 035006.

SRINIVASAN, K. & YOUNG, W. R. 2012 Zonostrophic instability. *J. Atmos. Sci.* **69** (5), 1633–1656.

THOMAS, V., FARRELL, B. F., IOANNOU, P. J. & GAYME, D. F. 2015 A minimal model of self-sustaining turbulence. *Phys. Fluids* **27**, 105104.

THOMAS, V., LIEU, B. K., JOVANOVIĆ, M. R., FARRELL, B. F., IOANNOU, P. J. & GAYME, D. F. 2014 Self-sustaining turbulence in a restricted nonlinear model of plane Couette flow. *Phys. Fluids* **26**, 105112.

TOH, S. & ITANO, T. 2005 Interaction between a large-scale structure and near-wall structures in channel flow. *J. Fluid Mech.* **524**, 249–262.

TOWNSEND, A. A. 1976 *The structure of turbulent shear flow*, 2nd edn. Cambridge University Press.